International Journal of Nanomedicine

Dovepress
Taylor & Francis Group

Open Access Full Text Article

ORIGINAL RESEARCH

Primed Extracellular Vesicles as a Nanotherapeutic Strategy to Enhance Granulosa Cell Function in a Model of Premature Ovarian Insufficiency and Hormonal Decline

Ju-Sheng Shieh[1,*], Yu-Tang Chin[1,2,*], Jiong Jiong Guo[3,4], Hsien-Chung Chiu[2], Hui-Rong Cheng[2], Hung-Han Hsu[2], Chuang-Yen Huang[2,5,6], Yu-Hsuan Chen[2,5], Ya-Yu Hsieh[7], Fung-Wei Chang[2,8]

[1]Department of Periodontology, School of Dentistry, Tri-Service General Hospital and National Defense Medical University, Taipei City, Taiwan; [2]Department of Obstetrics and Gynecology, Tri-Service General Hospital and National Defense Medical University, Taipei City, Taiwan; [3]Department of Orthopedics and Sports Medicine, The First Affiliated Hospital of Soochow University, Suzhou, Jiangsu, People's Republic of China; [4]MOE China-Europe Sports Medicine Belt and Road Joint Laboratory, Soochow University, Suzhou, Jiangsu, People's Republic of China; [5]Division of Obstetrics and Gynecology, Tri-Service General Hospital Penghu Branch, National Defense Medical University, Penghu, Taiwan; [6]Graduate Institute of Medical Sciences, National Defense Medical University, Taipei City, Taiwan; [7]Department and Graduate Institute of Pharmacology, College of Medicine, National Taiwan University, Taipei City, Taiwan; [8]Department of Obstetrics and Gynecology, Taipei City Hospital, Taipei, Taiwan

*These authors contributed equally to this work

Correspondence: Fung-Wei Chang, Department of Obstetrics and Gynecology, Tri-Service General Hospital, National Defense Medical University, No. 325, Sec.2, Chenggong Road, Neihu District, Taipei City, 11490, Taiwan, Email doc30666@gmail.com

Background: Premature ovarian insufficiency (POI) is characterized by granulosa cell (GC) dysfunction, reduced steroidogenesis, and hypoestrogenism, often secondary to chemotherapy. Despite advancements in regenerative medicine, cell-free nanotherapies remain underexplored for POI treatment.

Purpose: This study investigates the therapeutic efficacy of primed avian mesenchymal stem cell-derived small extracellular vesicles (primed AMSC-sEVs) in a cyclophosphamide (CTX)-induced GC injury model, mimicking POI-associated hormonal dysfunction.

Methods: Primed AMSC-sEVs were characterized in terms of particle size, concentration, and zeta potential using the Exoid TRPS and electrophoretic mobility platforms. Functional comparisons between primed and naïve AMSC-sEVs were conducted in human granulosa cells (hGCs), evaluating cell viability, apoptosis, steroidogenesis, and ovarian function-associated gene expression. miRNA content was assessed by next-generation sequencing and qRT-PCR.

Results: Primed AMSC-sEVs displayed a smaller, more uniform size distribution, significantly enhanced particle concentration, and greater negative zeta potential (mean −24.4 mV vs −13.3 mV), suggesting improved colloidal stability. In vitro, primed sEVs dose-dependently enhanced hGC proliferation, restored CTX-induced suppression of AMH, FSHR, and LHCGR, and elevated estradiol and progesterone levels. Apoptotic markers (cleaved Caspase-3, BAX, PARP) were reduced, while BCL-2 was upregulated. Key miRNAs involved in steroidogenic and apoptotic regulation (miR-21, miR-22, miR-23b, miR-145, miR-199a) were enriched in primed sEVs.

Conclusion: Primed AMSC-sEVs offer a promising nanotherapeutic strategy to restore ovarian cell function in POI-like conditions via enhanced anti-apoptotic and steroidogenic effects. These findings support the translational potential of Primed sEVs for fertility preservation and the management of menopausal hormone deficiency, including early-stage ovarian insufficiency and genitourinary syndrome of menopause.

Keywords: premature ovarian insufficiency, primed small extracellular vesicles, granulosa cells, anti-mullerian hormone, estradiol, progesterone, menopause

Received: 14 April 2025
Accepted: 31 August 2025
Published: 11 September 2025

Introduction

Ovarian aging is a progressive process that may begin well before the onset of menopause. Under pathological conditions, approximately 1% to 4% of women experience premature ovarian insufficiency (POI), a condition characterized by hypoestrogenism, menstrual irregularity, and reduced fertility. POI is broadly categorized as either primary or secondary. Primary POI is often idiopathic but has been associated with genetic abnormalities,[1] autoimmune disorders, chronic inflammation, and enzyme deficiencies.[2] Secondary POI may result from surgical interventions, radiotherapy, chemotherapy, or environmental toxin exposure.[3] Regardless of etiology, GC dysfunction plays a central role in the pathophysiology of POI. GCs are critical for follicular development, oocyte maturation, and steroid hormone production. Their premature depletion or apoptosis disrupts folliculogenesis and leads to hormonal insufficiency. While high-dose chemotherapy and radiotherapy are known to adversely affect ovarian function in young women,[4] their effect on GCs—particularly via apoptosis—has provided a basis for modeling ovarian insufficiency in vitro.[5] Among these, low-dose cyclophosphamide (CTX) has been widely used to induce senescence and apoptosis in GCs, without directly targeting oocytes, thereby serving as a reproducible cellular model to mimic POI-associated ovarian dysfunction.[6,7] In this study, we utilized CTX-induced GC damage as a model to simulate the cellular impairments observed in POI. Rather than focusing solely on chemotherapy-induced ovarian failure, our aim was to evaluate therapeutic strategies capable of restoring GC viability and endocrine function more broadly. This approach supports the development of regenerative therapies applicable not only to POI but also to conditions characterized by hormonal decline, such as early ovarian aging and genitourinary syndrome of menopause (GSM).

Accumulating evidence indicates that specific microRNAs (miRNAs) play pivotal regulatory roles in GC steroidogenesis and are integral to the maintenance of ovarian endocrine function. These miRNAs modulate diverse pathways involved in cell survival, hormone biosynthesis, and follicular development. For instance, miR-21 has been shown to promote GC survival and enhance estradiol (E2) and progesterone (P4) production by suppressing apoptotic signaling pathways.[8,9] MiR-22 regulates the expression of aromatase, a key enzyme in estrogen biosynthesis, thereby contributing to hormonal balance.[9,10] MiR-23b influences steroidogenic output by modulating inflammatory signaling and luteinizing hormone receptor (LHR) expression, with downstream effects on progesterone production.[10] Additionally, miR-145 regulates the expression of steroidogenic enzymes and facilitates cholesterol transport, both essential for steroid hormone synthesis.[10] MiR-199a supports follicular maturation and steroidogenesis, ensuring appropriate levels of E2 and P4 during follicle development.[11] A deeper understanding of these miRNA-mediated pathways is crucial for developing strategies to preserve or restore GC function under pathological conditions such as POI. Moreover, modulating specific miRNAs through extracellular vesicle-based delivery systems offers a promising direction for non-hormonal, cell-free therapies targeting ovarian insufficiency.

Mesenchymal stem cells (MSCs) have demonstrated therapeutic potential in promoting follicular regeneration and GC repair; however, their clinical application is hindered by challenges such as immune rejection, tumorigenic risk, limited donor availability, and ethical considerations.[12] As a cell-free alternative, extracellular vesicles (EVs) derived from MSCs have gained increasing attention due to their low immunogenicity, non-tumorigenic nature, and favorable safety profile.[13] EVs are lipid bilayer-enclosed nanostructures secreted by cells that mediate intercellular communication through the transfer of bioactive molecules, including mRNA, miRNA, circRNA, lncRNA, and proteins. They play essential roles in diverse physiological processes such as embryonic development, gametogenesis, and folliculogenesis. Notably, studies have shown that MSC-derived EVs can restore estrous cycles, increase follicle numbers, and suppress GC apoptosis in POI models, although the underlying mechanisms remain incompletely understood.[13]

According to the International Society of Extracellular Vesicles (ISEV), EVs are classified based on their size and biogenesis into apoptotic bodies (50–2000 nm), microvesicles (150–1000 nm), and exosomes (30–150 nm), with small EVs (sEVs, <200 nm) emerging as a particularly attractive therapeutic modality due to their favorable size, intrinsic targeting ability, and capacity for membrane fusion and cargo delivery.[14,15] Compared to synthetic nanoparticles, sEVs offer superior biocompatibility and efficiency in delivering functional regulatory molecules, particularly miRNAs, positioning them as promising nanotherapeutic carriers.[16–18] However, the biological activity of sEVs can vary depending on the physiological state or stimulation conditions of the parent MSCs. Increasing evidence indicates that EVs

derived from primed or induced MSCs contain higher levels of therapeutic metabolites and regulatory RNAs, leading to enhanced reparative efficacy.[19] These findings underscore the importance of upstream cell conditioning in optimizing the regenerative potential of sEVs and support the development of next-generation, functionally tailored extracellular vesicles for ovarian restoration and hormonal regulation.

Building upon these findings, our previous study demonstrated that sEVs derived from avian mesenchymal stem cells (AMSCs), when Primed with *Polygonum multiflorum* Thunb (PM) extract—a traditional Chinese medicinal herb historically used for aging-related conditions—exhibited enhanced regenerative potential. Specifically, these primed AMSC-sEVs significantly improved the bioactivity of skin fibroblasts and hair follicle cells, indicating their potential in tissue repair and cellular rejuvenation.[20] In addition to dermatological applications, the active constituent of PM extract, 2,3,5,4'-Tetrahydroxystilbene-2-O-β-D-Glucoside, has been reported to exert beneficial effects on female reproductive health. Experimental studies have shown that PM extract may enhance oocyte quality and yield, delay ovarian aging, and upregulate genes associated with mitochondrial biogenesis and steroidogenesis, thereby supporting ovarian reserve and endocrine function.[21] These findings suggest that PM-derived bioactives could modulate key molecular pathways involved in ovarian homeostasis and fertility preservation.

In this study, we hypothesized that primed AMSC-sEVs incorporating PM-derived signals could exert therapeutic effects on GCs under stress conditions resembling POI. Using a CTX-induced in vitro POI-like model, we aimed to investigate whether primed sEVs could restore GC viability, suppress apoptosis, and enhance steroidogenic function. Furthermore, we compared the biological effects of primed sEVs with naïve AMSC-sEVs to determine the added value of priming in augmenting sEV therapeutic efficacy.

Materials and Methods

Reagents and Cell Lines

Lyophilized primed and naïve avian mesenchymal stem cell-derived small extracellular vesicles (primed AMSC-sEVs and naïve AMSC-sEVs) were prepared as previously described[20] and supplied by Ascension Medical Biotechnology CO., LTD. (Taipei City, Taiwan). The priming process involved stimulation of AMSCs with *Polygonum multiflorum* extract under defined conditions to enhance extracellular vesicle production and cargo enrichment.[20] Enzyme-linked immunosorbent assay (ELISA) kits for estradiol (E2; Item No. 501890) and progesterone (P4; Item No. 582601) were obtained from Cayman Chemical (Ann Arbor, MI, USA). Human granulosa cells (HGL5/hGCs) were procured from Applied Biological Materials Inc. (Richmond, BC, Canada). The HGL5 cell line is an immortalized GC model established by transfection of primary human GCs with Simian Virus 40 (SV40) large T-antigen, which enables extended proliferation while preserving key GC phenotypes. These cells retain the expression of critical ovarian markers, including follicle-stimulating hormone receptor (FSHR), luteinizing hormone/choriogonadotropin receptor (LHCGR), and anti-Müllerian hormone (AMH), and are widely utilized in reproductive biology research to investigate steroidogenesis, follicular signaling, and gonadotropin responsiveness.

AMSC-sEV Production, Priming, and Isolation

The sEVs used in this study were derived from AMSCs and subjected to a priming process using *Polygonum multiflorum* Thunb. extract under serum-free, chemically defined conditions, as previously described in detail.[20] Briefly, AMSCs were exposed to the botanical priming agent for 48 hours, after which conditioned medium was harvested for sEV isolation.

The isolation and concentration of sEVs followed a standardized protocol involving sequential low-speed centrifugation, filtration through 0.45 μm and 0.22 μm membranes, tangential flow filtration (TFF), and ultrafiltration using 100 kDa MWCO centrifugal filters. Final products were lyophilized under sterile conditions for long-term storage and reconstituted in PBS prior to use. The physicochemical properties, surface charge, and vesicle morphology were previously validated in the cited reference.[20]

Particle Size Distribution and Zeta Potential

The particle size and concentration of naïve and primed AMSC-sEVs were assessed using tunable resistive pulse sensing (TRPS) on the Exoid system (IZON Science, New Zealand). For each analysis, 50 mg of lyophilized vesicles were reconstituted in 500 µL phosphate-buffered saline (PBS) and filtered through 0.22 µm membranes to remove aggregates. Measurement protocols followed previously reported procedures.[20,22,23] Calibration was performed with standard beads (CPC100, IZON), and data were acquired using nanopore NP150. Zeta potential analysis was also conducted using the Exoid nanopore-based system, which enables high-resolution, single-particle electrophoretic mobility assessment. To optimize conductivity and signal resolution, all samples were diluted 11-fold in PBS and analyzed at room temperature. This dual approach provided comprehensive characterization of vesicle size, distribution profile, surface charge, and dispersion stability.

RNA Extraction and Next-Generation Sequencing

Total RNA was extracted from both naïve and primed AMSC-sEVs using the qEV RNA Extraction Kit (IZON, Christchurch, New Zealand), according to the manufacturer's instructions. RNA integrity and concentration were assessed using the Agilent Bioanalyzer 2100 (Agilent Technologies, USA) prior to library preparation, ensuring RNA integrity number (RIN) >7 before downstream processing. Small RNA libraries were constructed using the QIAseq miRNA Library Kit (Qiagen, Hilden, Germany). Unique molecular indices (UMIs) were incorporated during reverse transcription (RT) and PCR amplification to facilitate accurate and de-duplicated quantification of individual miRNA molecules.[24] Final libraries were quality-checked, pooled equimolarly, and subjected to high-throughput sequencing using the NovaSeq 6000 platform (Illumina, San Diego, CA, USA). Bioinformatic processing included adapter trimming, quality filtering (Phred score ≥30), and UMI-based duplicate removal. Cleaned reads were aligned against the miRBase, piRNAbank, and Rfam databases for annotation. Normalized miRNA expression values were calculated as counts per million (CPM), and statistical analysis was conducted using the EdgeR package.[10] Differentially expressed miRNAs (DEMs) were identified using $|\log_2$ fold change$| \geq 1$ and false discovery rate (FDR)-adjusted p-value < 0.05 as the threshold.

miRNA Quantitative RT-PCR Analysis

For qRT-PCR validation of selected miRNAs, total RNA was extracted from sEV samples using the Total RNA Purification Kit (Norgen Biotek Corp., Thorold, Ontario, Canada). RNA concentration was quantified using the Qubit™ RNA HS Assay Kit (Thermo Fisher Scientific Inc., Waltham, MA, USA). Reverse transcription was carried out using the TOOLS miRNA RT Kit (BIOTOOLS Co., Ltd., New Taipei City, Taiwan), followed by qPCR using TOOLS miRNA RT-qPCR probes and TOOLS Easy 2× Probe qPCR Mix. Quantitative PCR reactions were run on a QuantStudio™ 12K Flex Real-Time PCR System (Applied Biosystems, Waltham, MA, USA). Target miRNAs included gga-miR-21-5p, gga-miR-22-3p, gga-miR-22-5p, and gga-miR-199a-5p, with U6 and cel-miR-39-3p used as internal reference genes. The ΔCt method was used for normalization, and relative fold change was calculated using the $2^{-\Delta\Delta Ct}$ formula. All assays were performed in triplicate, and statistical significance was determined by two-tailed *Student's t*-test with $p < 0.05$ considered significant.

Cell Proliferation Assay

Human granulosa cells (hGCs) were used to assess cell viability, with experimental procedures approved by the Institutional Review Board of the Tri-Service General Hospital and National Defense Medical Center (TSGHIRB No. C202405116). Cells were cultured in standard growth medium until they reached approximately 80% confluence, then seeded into 96-well plates at a density of 5×10^3 cells per 100 µL per well. After seeding, plates were incubated at 37 °C with 5% CO_2 for 24 hours to allow for cell attachment. Subsequently, cells were washed once with phosphate-buffered saline (PBS; Thermo Fisher Scientific Inc.) and cultured overnight in medium containing 0.25% charcoal-stripped fetal bovine serum (FBS; Cat. No.: A3382101, Thermo Fisher Scientific Inc.) for starvation. Following starvation, cells were treated with primed AMSC-sEVs (1×10^4, 1×10^6, and 1×10^8 particles/mL), naïve AMSC-sEVs (1×10^8 particles/mL), and/

or cyclophosphamide (CTX; 0, 0.1, 1, 2, 5, and 10 μM, dissolved in DMSO) for a total of 4 days. Vehicle controls received an equivalent volume of PBS or DMSO. To examine the protective effect of sEVs on CTX-induced GC damage, a sequential two-phase treatment was conducted. First, hGCs were exposed to 2 μM CTX for 2 days to induce cellular damage. After this initial exposure, cells were treated with either primed AMSC-sEVs (1×10^4 or 1×10^8 particles/mL) or naïve AMSC-sEVs (1×10^8 particles/mL) for an additional 2 days. All treatments and media were replenished every other day. Following the completion of treatment, cell viability was evaluated using the Cell Counting Kit-8 (CCK-8; DOJINDO Laboratories, Japan). Culture medium was replaced with fresh medium containing 10% CCK-8 reagent, and cells were incubated for 2 hours at 37 °C. Absorbance at 450 nm was measured using a VersaMax ELISA microplate reader (Molecular Devices; San Jose, CA, USA).

Quantitative Real-Time Polymerase Chain Reaction

To evaluate gene expression changes following CTX and sEV treatments, quantitative real-time PCR (qRT-PCR) was performed on treated hGCs. After an overnight starvation period in medium containing 0.25% stripped FBS, hGCs were initially exposed to varying concentrations of CTX (0, 0.1, 1, 2, 5, and 10 μM) for 48 hours. This was followed by a 48-hour treatment phase with or without sEVs—either naïve or primed AMSC-derived sEVs—at doses of 1×10^4 or 1×10^8 particles/mL (dissolved in PBS). Total RNA was extracted using the Quick-RNA Miniprep Kit (Zymo Research Corporation, Irvine, CA, USA) with on-column DNase I treatment to eliminate genomic DNA contamination. Reverse transcription was performed using 0.5 μg of purified RNA and the PrimeScript™ RT Reagent Kit (Takara Bio Inc., Shiga, Japan), according to the manufacturer's instructions. The resulting complementary DNA (cDNA) was used as a template for qRT-PCR amplification using the QuantiFast SYBR Green PCR Kit (Qiagen, Hilden, Germany) on the Rotor-Gene Q Real-Time PCR Detection System (Qiagen). Thermal cycling conditions were as follows: initial denaturation at 95 °C for 5 minutes, followed by 45 cycles of denaturation at 95 °C for 10 seconds, and combined annealing and extension at 60 °C for 30 seconds. Primer sequences for target genes (*AMH, FSHR, LHCGR*, and others) were designed based on Homo sapiens reference sequences and are listed in Table 1. Relative gene expression was normalized to 18S rRNA as the internal control and calculated using the $2^{-\Delta\Delta CT}$ method. Amplification specificity was confirmed by melt curve analysis and single peak detection.

Western Blot Analysis

Western blotting was performed to evaluate the expression of apoptotic and anti-apoptotic proteins in hGCs following experimental treatments. Cells were harvested and lysed using radioimmunoprecipitation assay (RIPA) buffer supplemented with protease and phosphatase inhibitor cocktails (Bio-Rad Laboratories, Inc., Hercules, CA, USA). Protein concentrations were determined using the bicinchoninic acid (BCA) Protein Assay Kit (Thermo Fisher Scientific Inc., Waltham, MA, USA). Equal amounts of protein samples were resolved by SDS-PAGE using 4–20% Mini-PROTEAN® TGX™ Precast Protein Gels (Catalog No.: 4561093; Bio-Rad Laboratories, Inc.) and transferred onto nitrocellulose membranes (Bio-Rad Laboratories, Inc.) via wet transfer at 100 V for 60 minutes at 4 °C in transfer buffer (25 mM Tris base, 192 mM glycine, 20% methanol, pH 8.3). Membranes were blocked overnight at 4 °C in 5% non-fat dry milk

Table 1 Primer Sequences for Homo sapiens

Forward	Backward	Accession No.
GCCTTGCCCTCTCTACGGC	TGTTGGCTCCCAGGTCACTTC	NM_000479.5
GGAACCCAACTAGATGCAGTGA	CAGAGGCTCCGTGGAAAACA	M65085.1
GCCGTCCACTCGACTATCAC	TGAGGAGGTTGTCAAAGGCAT	M73746.1
TCTGAGGGCTTCGACACCTA	TCATTGCCGGCGCATTTTAG	BC062439.1
GATAACGGAGGCTGGGATGC	AGTCTTCAGAGACAGCCAGGA	NM_000633.3
AGGCGGTTGTAGAAGAGTTTCG	ACCCACCGAAAACCAGAGC	NM_004346.4
AAGTCTAGAGCCACCGTCCA	CAGTCTGGCTGCCAATCCA	NM_000546.5
GTAACCCGTTGAACCCCATT	CCATCCAATCGGTAGTAGCG	NR_003286

https://doi.org/10.2147/IJN.S533393

prepared in Tris-buffered saline with 0.1% Tween-20 and then incubated with primary antibodies against cleaved Caspase-3, cleaved Caspase-9, BAX, BCL-2, cleaved PARP, and β-actin (1:1000–1:3000; GeneTex International Corporation, Hsinchu, Taiwan) overnight at 4 °C. After washing, membranes were incubated with HRP-conjugated secondary antibodies (1:5000; GeneTex International Corporation) for 1 hour at room temperature. Protein bands were visualized using enhanced chemiluminescence reagents (Bio-Rad Laboratories, Inc.) and imaged with the ChemiDoc™ XRS+ Imaging System (Bio-Rad Laboratories, Inc). Densitometric analysis was performed using Image Lab Software (Bio-Rad Laboratories, Inc)., and target protein expression levels were normalized to β-actin as the internal control.

Annexin-V and Propidium Iodide Staining

To evaluate the effect of sEV treatment on CTX-induced apoptosis in hGCs, cell death was assessed using the Alexa Fluor 488-conjugated Annexin V and propidium iodide (PI) apoptosis detection kit (Thermo Fisher Scientific Inc., Waltham, MA, USA), following the manufacturer's instructions. Briefly, after treatment with CTX and/or sEVs, cells were harvested by trypsinization, washed with DPBS (Thermo Fisher Scientific Inc)., and resuspended in 100 µL of binding buffer (50 mM HEPES, 700 mM NaCl, 12.5 mM $CaCl_2$, pH 7.4) per 1×10^6 cells. Annexin V and PI were added directly to the cell suspension, and samples were incubated for 15 minutes at room temperature in the dark. After staining, samples were diluted with 0.4 mL of binding buffer per million cells and analyzed immediately using a FACSCalibur™ flow cytometer (BD Biosciences, Franklin Lakes, NJ, USA). Data acquisition and analysis were performed using CellQuest™ Pro or FlowJo version 10 software (BD Biosciences), collecting either 10,000 or 50,000 events per sample. Fluorescence signals were detected using a 488 nm laser. PI fluorescence was collected through a 650LP filter, while Annexin V-Alexa Fluor 488 fluorescence was measured using a 530 nm filter. The percentage of apoptotic cells was calculated as the sum of PI^+/Annexin V^+ (late apoptotic/necrotic) and PI^-/Annexin V^+ (early apoptotic) populations, divided by the total number of cells. Due to the minimal presence of Annexin V^+/PI^- single-positive cells in most experimental conditions, data interpretation was primarily based on the combined PI^+ and double-positive populations.

Immunofluorescence Staining and Laser Scanning Confocal Microscopy

hGCs were cultured on dual-chambered slides (Thermo Fisher Scientific Inc.) and fixed with 4% paraformaldehyde for 10 minutes at room temperature. Cells were permeabilized using 0.2% Triton X-100 (Merck, Burlington, MA, USA) for 5 minutes. Slides were either processed immediately or air-dried for 5 minutes and stored at −80 °C until further analysis. For immunostaining, slides were re-permeabilized with pre-chilled 50:50 acetone:methanol solution (−20 °C) for 20 minutes. After washing, samples were blocked in PBS containing 10% FBS and 1% bovine serum albumin for 1 hour at 37 °C. Cells were then incubated overnight at 4 °C with a rabbit polyclonal anti-anti-Müllerian hormone (AMH) antibody (GTX129593, GeneTex International Corporation, Hsinchu, Taiwan) diluted 1:500 in blocking buffer. The following day, slides were washed and incubated for 1 hour at 37 °C in the dark with DyLight 488-conjugated goat anti-rabbit IgG secondary antibody (1:1000; GeneTex International Corporation). After final washes, slides were mounted with EverBrite™ Hardset Mounting Medium containing DAPI (Biotium, Inc., Fremont, CA, USA). Fluorescence images were acquired using a Carl Zeiss LSM 880 laser scanning confocal microscope (Carl Zeiss, Oberkochen, Germany) at room temperature. To ensure data consistency, images used for comparative analysis across treatment groups were captured under identical acquisition settings and exposure times. Post-acquisition processing was limited to whole-image adjustments and conducted using Adobe Photoshop 6.0 (Adobe Systems, San Jose, CA, USA). Quantitative analysis of AMH fluorescence intensity was performed using ImageJ software (https://imagej.net/ij/).

Hormone Assays

The concentrations of estradiol (E2) and progesterone (P4) in the culture supernatants of treated hGCs were quantified using commercially available ELISA kits specific for human E2 (Ann Arbor, MI, USA) and P4 (Cayman Chemical). The E2 ELISA kit featured a dynamic detection range of 0.61–10,000 pg/mL and a sensitivity of approximately 20 pg/mL at 80% B/B_0. The P4 assay had a measurement range of 7.8–1,000 pg/mL, with a sensitivity of approximately 10 pg/mL at 80% B/B_0. Both assays exhibited intra-assay and inter-assay coefficients of variation (CVs) below 12%, ensuring

analytical reliability. Hormone concentrations were calculated according to the manufacturers' protocols using standard curves and were reported as pg/mL for E2 and ng/mL for P4.

Statistical Analysis

All quantitative data, including cell viability, gene expression, protein expression, and hormone levels, were analyzed using IBM SPSS Statistics version 19.0 (SPSS Inc., Chicago, IL, USA). For comparisons involving more than two groups, one-way analysis of variance (ANOVA) followed by *Duncan's post hoc* test was applied to determine statistical significance. The significance threshold was set at $p < 0.05$. Significance levels were denoted as follows: * / # / $ for $p < 0.05$; ** / ## / $$ for $p < 0.01$; and *** / ### / $$$ for $p < 0.001$. Each symbol represents comparisons versus different control groups, as indicated in the figure legends.

Results

Primed AMSC-sEVs Exhibit Enhanced Physicochemical Properties and Significantly Promote hGC Proliferation

The physicochemical characteristics of naïve and primed AMSC- sEVs were analyzed using the TRPS system (Figure 1A). Compared with naïve sEVs, primed AMSC-sEVs showed a significantly higher particle concentration and a narrower, more uniform size distribution, indicating enhanced biogenesis and homogeneity following priming treatment. Notably, the average particle diameter of primed sEVs was smaller than that of naïve sEVs, suggesting structural refinement associated with the priming process.

In addition, zeta potential analysis revealed a substantial shift in surface charge following priming. Naïve sEVs displayed moderately negative zeta potentials (mean –13.0 to –13.3 mV; modal –4.9 to –7.5 mV), while primed sEVs exhibited markedly enhanced negative surface charges (mean –22.8 to –24.4 mV; modal –24.2 to –24.5 mV) (Figure 1B). This shift suggests improved colloidal stability and more homogeneous surface properties in the primed sEV population, potentially favoring cellular interaction and uptake.

To investigate the biological effects of primed sEVs, hGC cells were treated with either naïve or primed AMSC-sEVs at various concentrations for 96 hours. Cell proliferation analysis showed that both naïve and primed sEVs significantly promoted hGC proliferation, with naïve sEVs at 1×10^8 particles/mL inducing a modest but statistically significant increase compared to untreated controls ($p < 0.05$). Notably, primed sEVs induced a significantly greater proliferative response ($p < 0.001$) than naïve sEVs at equivalent particle concentrations (1×10^8/mL) (Figure 1C). Moreover, a dose-dependent effect was observed in the primed sEV group, further supporting their enhanced biological activity.

Primed AMSC-sEVs Ameliorate CTX-Induced in vitro POI of hGCs

To establish an in vitro POI model, hGCs were treated with various dosages (0, 0.1, 1, 2, 5, and 10 μM) of CTX for 48 hours to induce apoptosis. CTX significantly and dose-dependently reduced cell viability of hGCs ($p < 0.001$) (Figure 2A). Furthermore, to confirm whether the in vitro POI model of hGCs was successfully established by CTX treatment, the gene expressions of *AMH, FSHR*, and *LHCGR* were investigated. CTX treatment significantly and dose-dependently inhibited the gene expression of *AMH* at doses of 1, 2, 5, and 10 μM ($p < 0.001$) (Figure 2B). However, the gene expressions of *FSHR* and *LHCGR* were only significantly inhibited in hGCs following CTX treatment ($p < 0.001$) (Figure 2B).

To evaluate the ameliorative effect of primed AMSC-sEVs on a CTX-induced in vitro POI model of hGCs, a CTX concentration of 2 μM was applied. After a 48-hour pre-treatment with 2 μM CTX, the cells were then treated with AMSC-sEVs for an additional 48 h. primed AMSC-sEVs (10^8 particles/mL) not only significantly enhanced the cell proliferation of hGCs but also significantly ameliorated CTX-reduced cell proliferation ($p < 0.001$) (Figure 3A). To confirm if primed AMSC-sEVs attenuated CTX-induced apoptosis in hGCs, the percentage of apoptotic cells was measured. Treatment with 2 μM CTX significantly elevated the percentage of apoptotic hGCs ($p < 0.001$). However,

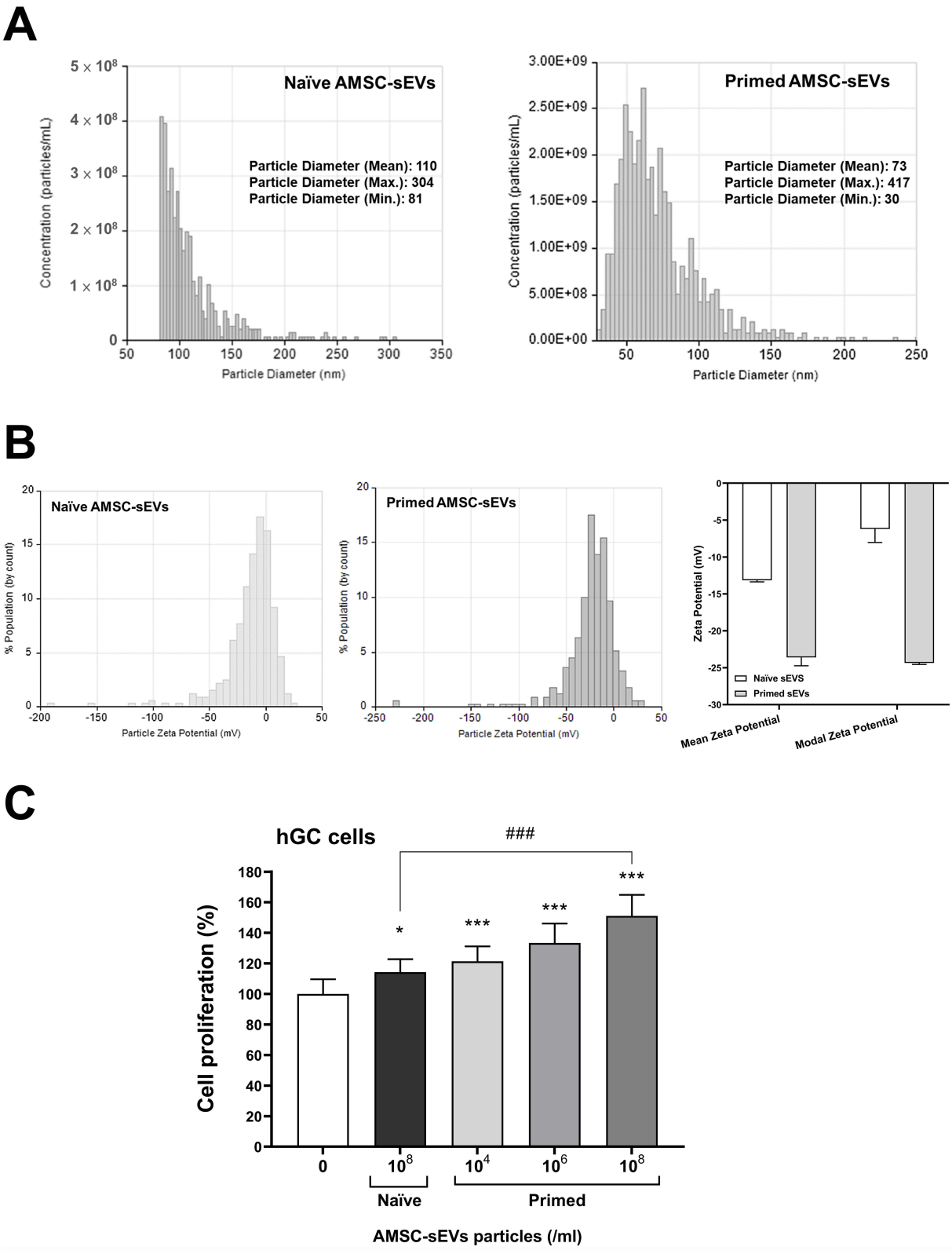

Figure 1 Characterization and functional analysis of naïve and Primed AMSC-sEVs. (**A**) Particle concentration and size distribution of naïve and Primed AMSC-sEVs measured by tunable resistive pulse sensing (TRPS) using the Exoid system. (**B**) Zeta potential of naïve and Primed AMSC-sEVs measured using the Exoid nanopore-based platform. All samples were diluted in 1× ME buffer prior to analysis. (**C**) The effect of Primed AMSC-sEVs on hGC cell proliferation, with hGCs treated for 96 h with naïve AMSC-sEVs and various concentrations of Primed AMSC-sEVs. (N = 6, data are expressed as the mean ± standard deviation; *$p < 0.05$, ***$p < 0.001$, compared with 0 particles/mL; $^{###}$ $p < 0.001$, compared with naïve AMSC-sEVs).

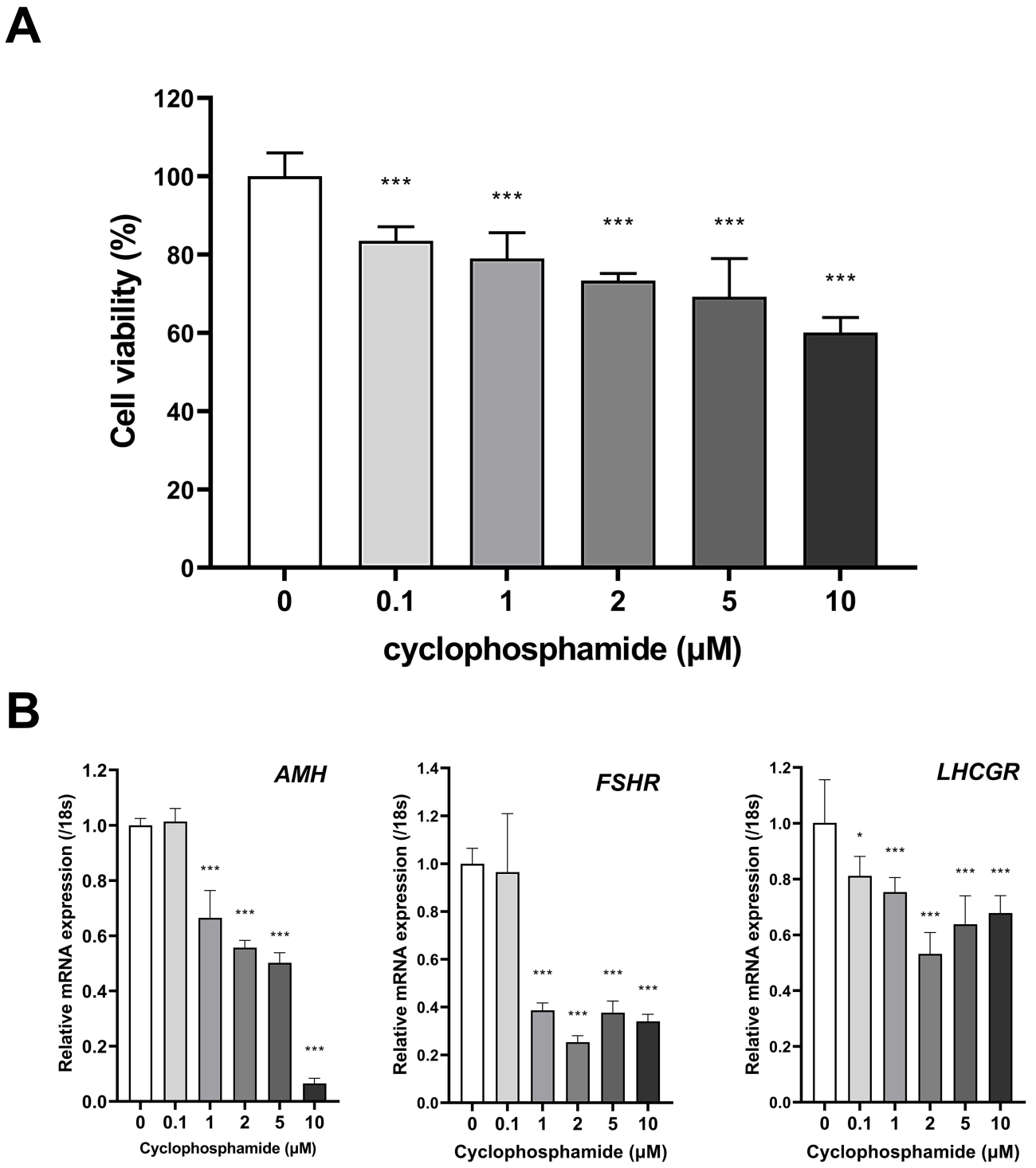

Figure 2 CTX-induced POI in an in vitro model. (**A**) The cell viability of hGCs after treated with various doses of cyclophosphamide (CTX) for 48 h. (**B**) The expressions of ovarian function-associated gene *AMH, FSHR*, and *LHCGR* were analyzed by qRT-PCR after 48h of CTX treatment. (N = 6, data are expressed as the mean ± standard deviation; *$p < 0.05$, ***$p < 0.001$, compared with 0 μM).

treatment with AMSC-sEVs significantly reduced the percentage of apoptotic hGCs ($p < 0.05$ without CTX treatment; $p < 0.001$ with CTX treatment), irrespective of whether CTX treatment was applied (Figure 3B). Furthermore, primed AMSC-sEVs diminished CTX-induced apoptosis in a dose-dependent manner and significantly decreased the percentage of apoptotic hGCs more effectively than naïve AMSC-sEVs at the same particle concentration (10^8/mL) ($p < 0.001$).

https://doi.org/10.2147/IJN.S533393

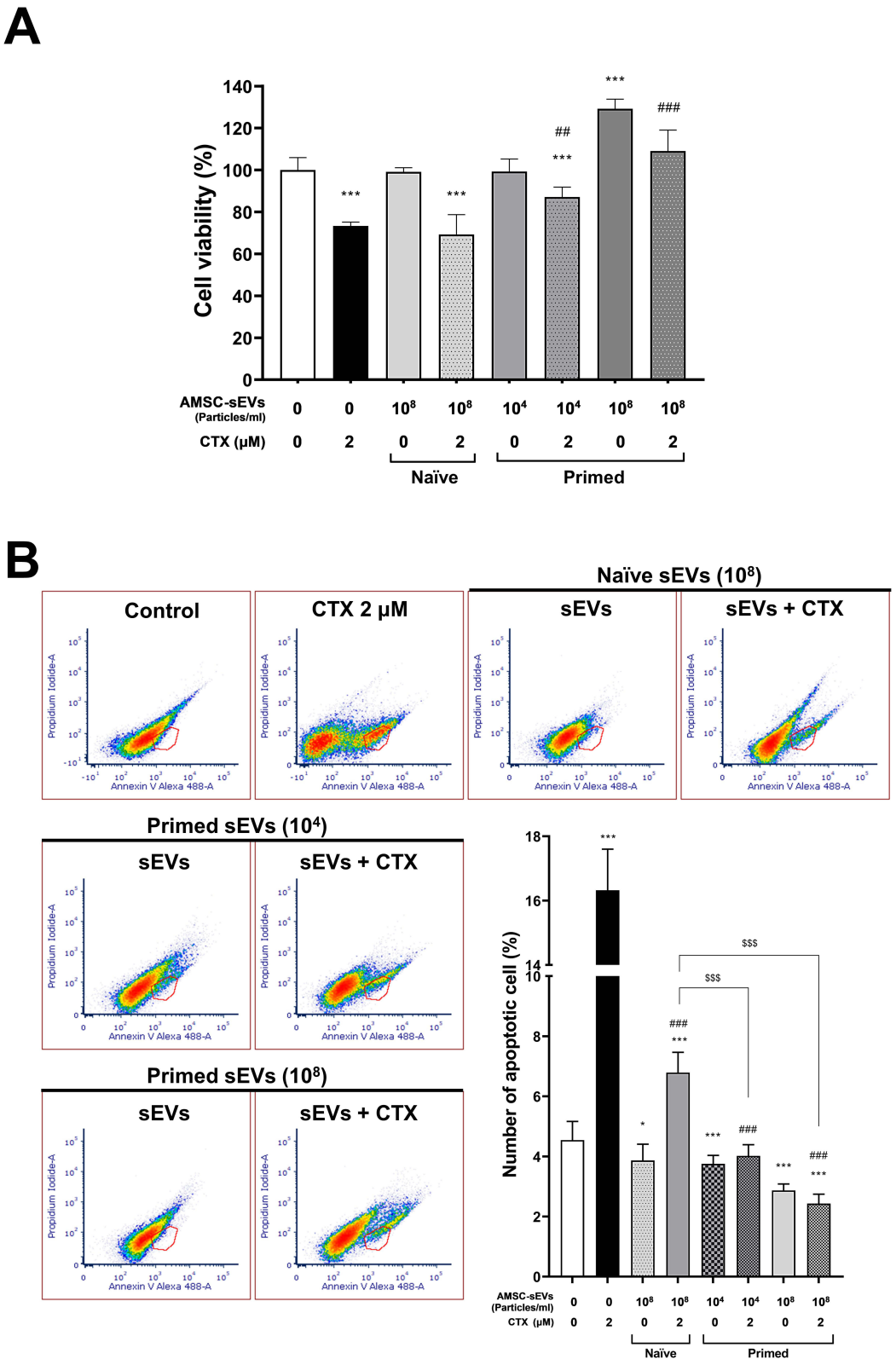

Figure 3 Primed AMSC-sEVs ameliorate CTX-induced POI in an in vitro model. (**A**) hGCs were treated with or without 2 μM CTX for 48 h, followed by treatment with naïve or Primed AMSC-sEVs for an additional 48 h. Cell viability was analyzed using CCK-8 assay. (**B**) The percentage of apoptotic hGCs was determined by Annexin-V and propidium iodide staining, followed by flow cytometry. Red circles indicate apoptotic cell populations ("A" region), as defined in the manufacturer's instructions, encompassing both early (Annexin V^+/PI^-) and late apoptosis (Annexin V^+/PI^+) quadrants. (N = 6, data are expressed as the mean ± standard deviation; $^*p < 0.05$, $^{***}p < 0.001$, compared with 0 μM and/or 0 particles/mL; $^{\#\#}p < 0.01$, $^{\#\#\#}p < 0.001$, compared with CTX 2 μM; $^{\$\$\$}p < 0.001$, compared with naïve AMSC-sEVs after CTX 2 μM treatment; Statistical indicators apply to both (**A**) and (B).).

Primed AMSC-sEVs Improve CTX-Disrupted Cell Activities of hGCs

To evaluate the restorative effect of primed AMSC-sEVs on CTX-disrupted cell activities in the in vitro POI model of hGCs, particularly focusing on ovarian function-associated, cell proliferative, and apoptotic/anti-apoptotic gene expressions, qRT-PCR analysis was conducted. Treatment with 2 μM CTX significantly reduced the expressions of ovarian function-associated gene *AMH, FSHR*, and *LHCGR* in hGCs ($p < 0.001$) (Figure 4A). Treatment with naïve AMSC-sEVs significantly enhanced the expression of *AMH* only ($p < 0.01$), whereas primed AMSC-sEVs augmented the expressions of *AMH, FSHR*, and *LHCGR* at the same particle concentration (10^8/mL) ($p < 0.001$) (Figure 4A). Furthermore, treatment with naïve AMSC-sEVs significantly restored the CTX-reduced expressions of *AMH* and *LHCGR* ($p < 0.001$), but not *FSHR*. Interestingly, primed AMSC-sEVs not only significantly restored these CTX-reduced gene expressions ($p < 0.001$) but also enhanced their expression levels beyond those of the control group ($p < 0.001$) (Figure 4A).

Regarding CTX-reduced cell proliferative (*PCNA*) and apoptotic (*TP53* and *CASP3*)/anti-apoptotic (*BCL-2*) gene expressions, treatment with naïve AMSC-sEVs did not enhance these gene expressions but did restore their CTX-reduced levels ($p < 0.001$) (Figure 4B). However, treatment with primed AMSC-sEVs not only significantly and dose-dependently enhanced the expressions of *PCNA* and *BCL-2* but also significantly reduced the expressions of *TP53* and *CASP3* ($p < 0.001$). Expectedly, primed AMSC-sEVs significantly restored the CTX-affected gene expressions in hGCs ($p < 0.001$) (Figure 4B).

Primed AMSC-sEVs Regulate Apoptotic Pathways to Protect hGCs from CTX-Induced Damage

Western blot analysis revealed that CTX exposure increased the expression of pro-apoptotic markers including cleaved Caspase-3, Caspase-8, Caspase-9, BAX, and cleaved PARP, whereas post-treatment with primed AMSC-sEVs led to a marked reduction in these proteins and upregulation of anti-apoptotic BCL-2 expression (Figure 5A). Compared to the control group, both naïve and primed AMSC-sEVs significantly reduced the cleavage of Caspase-3 ($p < 0.001$) and Caspase-9 ($p < 0.001$), indicating a suppression of apoptosis (Figure 5B). Notably, primed AMSC-sEVs exhibited a greater inhibitory effect on Caspase-9 cleavage than naïve AMSC-sEVs ($p < 0.001$), with statistical comparisons indicating a significant reduction compared to the naïve sEV group under the same CTX condition. Additionally, full-length PARP expression was preserved, while cleaved PARP was significantly downregulated in primed AMSC-sEVs-treated cells ($p < 0.001$) (Figure 5B). The pro-apoptotic protein BAX was significantly downregulated ($p < 0.001$), whereas the anti-apoptotic protein BCL-2 was significantly upregulated ($p < 0.001$), suggesting a shift toward cell survival (Figure 5B). Furthermore, primed AMSC-sEVs demonstrated a more pronounced effect in reducing BAX expression compared to naïve AMSC-sEVs (with $^{\$\$\$}$ indicating statistical significance under matched CTX treatment). The expression of Caspase-8 remained unchanged across all groups, indicating that primed AMSC-sEVs primarily modulate the intrinsic apoptotic pathway (Figure 5A).

Primed AMSC-sEVs Stimulate and Restore CTX-Reduced Steroidogenesis in hGCs

The elevation of ovarian function-associated genes by primed AMSC-sEVs treatment was observed. To confirm the protein expression of AMH after treatment with CTX, with or without AMSC-sEVs, in hGCs, confocal laser scanning microscopy was conducted. Results showed that the basal expression of AMH in hGCs was low, and CTX significantly affected AMH expression ($p < 0.01$) (Figure 6A and Supplementary Figure 1). Treatment with AMSC-sEVs significantly enhanced AMH expression in hGCs ($p < 0.05$ for naïve and $p < 0.001$ for primed), with primed AMSC-sEVs significantly showing a greater increase in AMH expression compared to naïve ones ($p < 0.001$). Additionally, primed AMSC-sEVs more effectively and significantly restored CTX-reduced AMH expression compared to naïve AMSC-sEVs ($p < 0.001$) (Figure 6A).

The effect of AMSC-sEVs on CTX-affected steroidogenesis in hGCs was also evaluated. The secretion of E2 and P4 was measured by ELISA. Treatment with 2 μM CTX significantly reduced E2 and P4 secretion in hGCs ($p < 0.001$) (Figure 6B and C). Naïve AMSC-sEVs did not affect the secretion of E2 and P4 in CTX-treated hGCs, but they significantly restored the CTX-reduced secretion of these hormones ($p < 0.001$). Furthermore, primed AMSC-sEVs not only

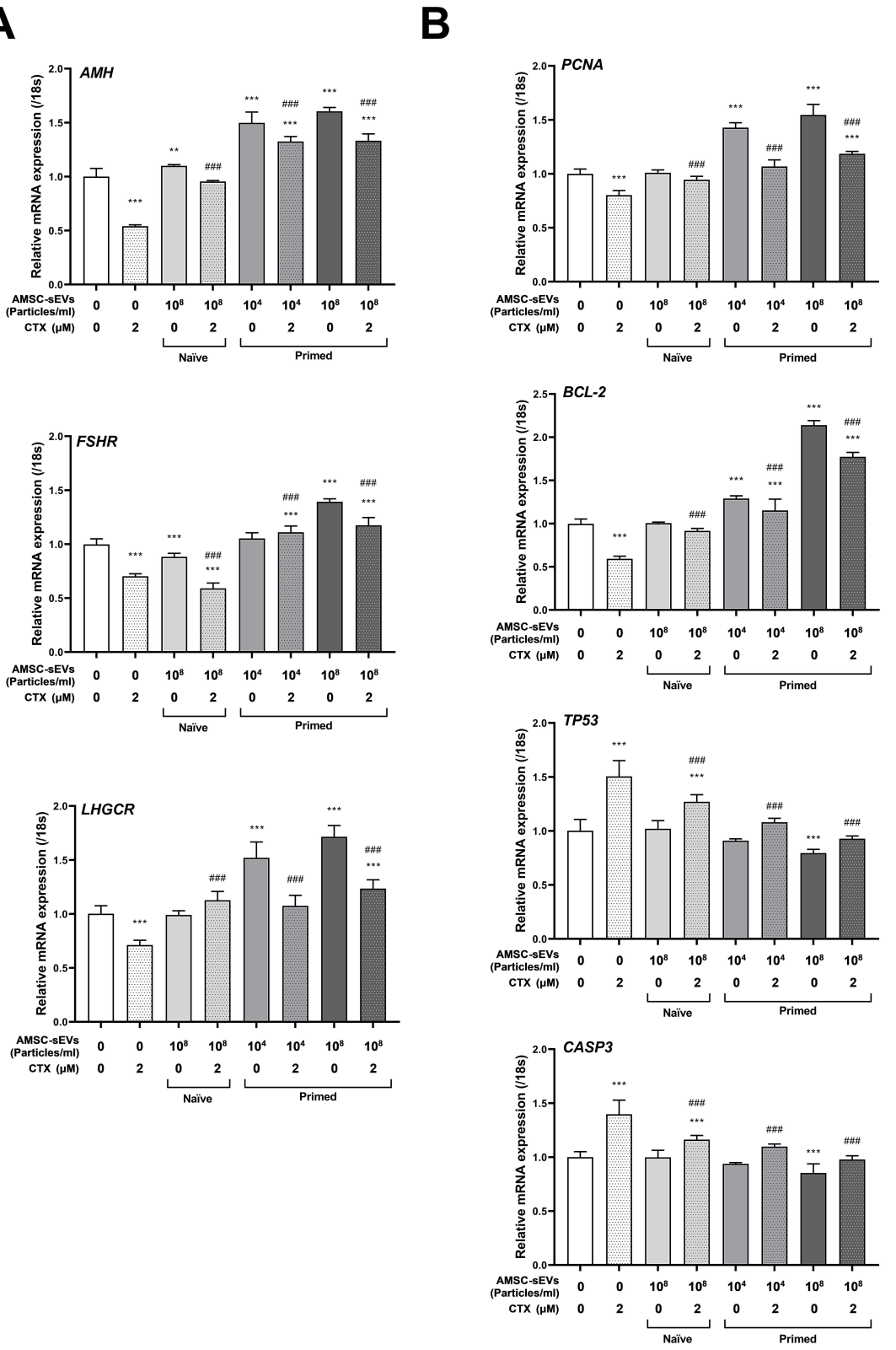

Figure 4 Primed AMSC-sEVs enhance CTX-disrupted cell activities in hGCs. hGCs were treated with or without 2 μM CTX for 48 h, followed by treatment with naïve or Primed AMSC-sEVs for an additional 48 h. (**A**) The expressions of ovarian function-associated gene *AMH, FSHR*, and *LHCGR* were analyzed by qRT-PCR. (**B**) The expressions of proliferative (*PCNA*), apoptotic (*TP53* and *CASP3*), and anti-apoptotic (*BCL-2*) gene expressions were also examined by qRT-PCR. (N = 6, data are expressed as the mean ± standard deviation; *$p < 0.05$, **$p < 0.01$, ***$p < 0.001$, compared with 0 μM and 0 particles/mL; ###$p < 0.001$, compared with CTX 2 μM).

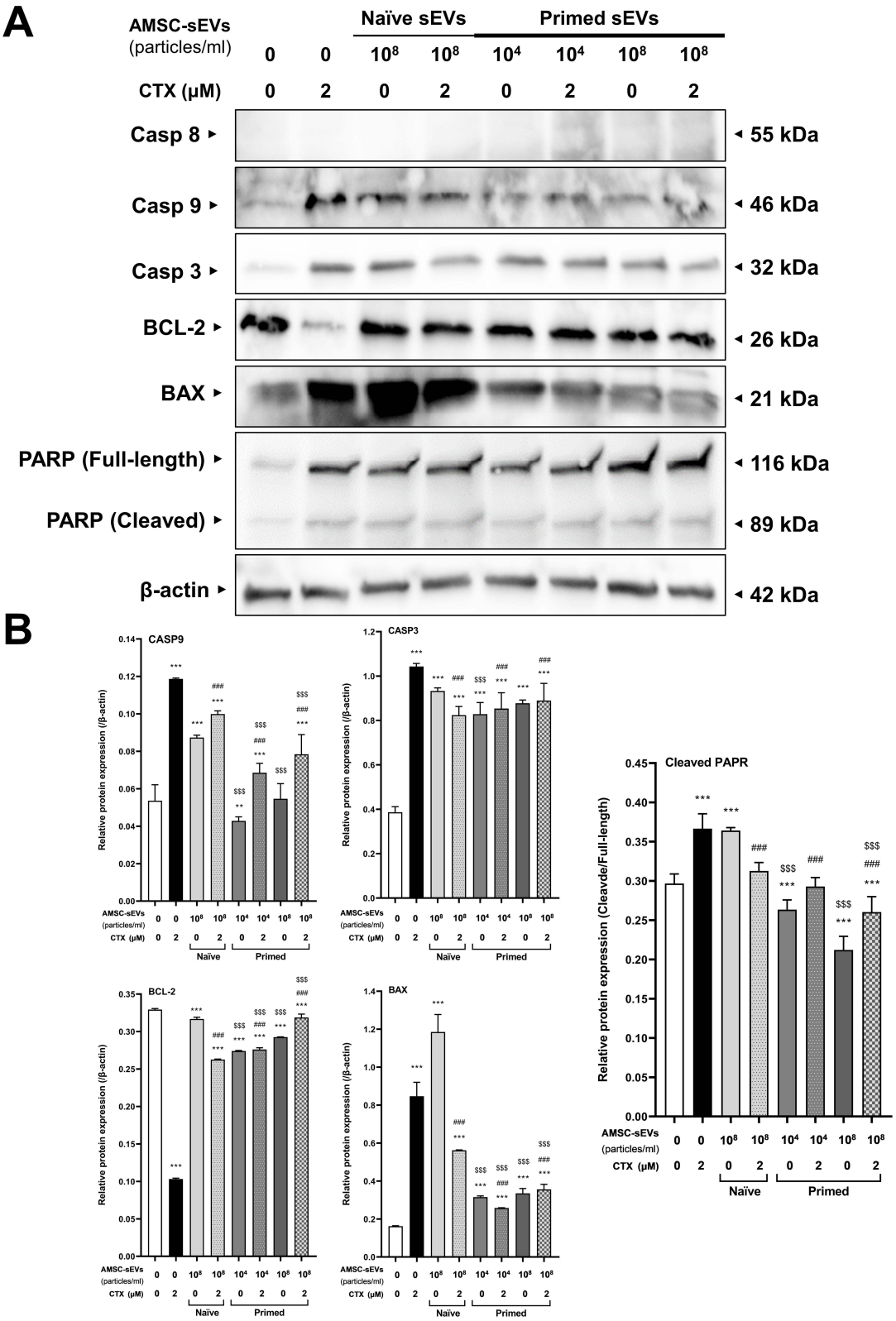

Figure 5 Primed AMSC-sEVs suppress apoptosis in CTX-treated hGCs. Western blot analysis of apoptosis-related proteins in CTX-treated hGCs following treatment with naïve AMSC-sEVs and Primed AMSC-sEVs. (**A**) Representative Western blot images showing the expression levels of cleaved Caspase-3, cleaved Caspase-9, cleaved PARP, BAX, BCL-2, and Caspase-8, with β-actin as a loading control. (**B**) Quantification of protein expression levels, normalized to β-actin. (N = 3, data are expressed as the mean ± standard deviation; ** $p < 0.01$, *** $p < 0.001$, compared with 0 μM and 0 particles/ml; ### $p < 0.001$, compared with CTX 2 μM; $$$ $p < 0.001$, compared with naïve AMSC-sEV group under the same CTX condition).

https://doi.org/10.2147/IJN.S533393

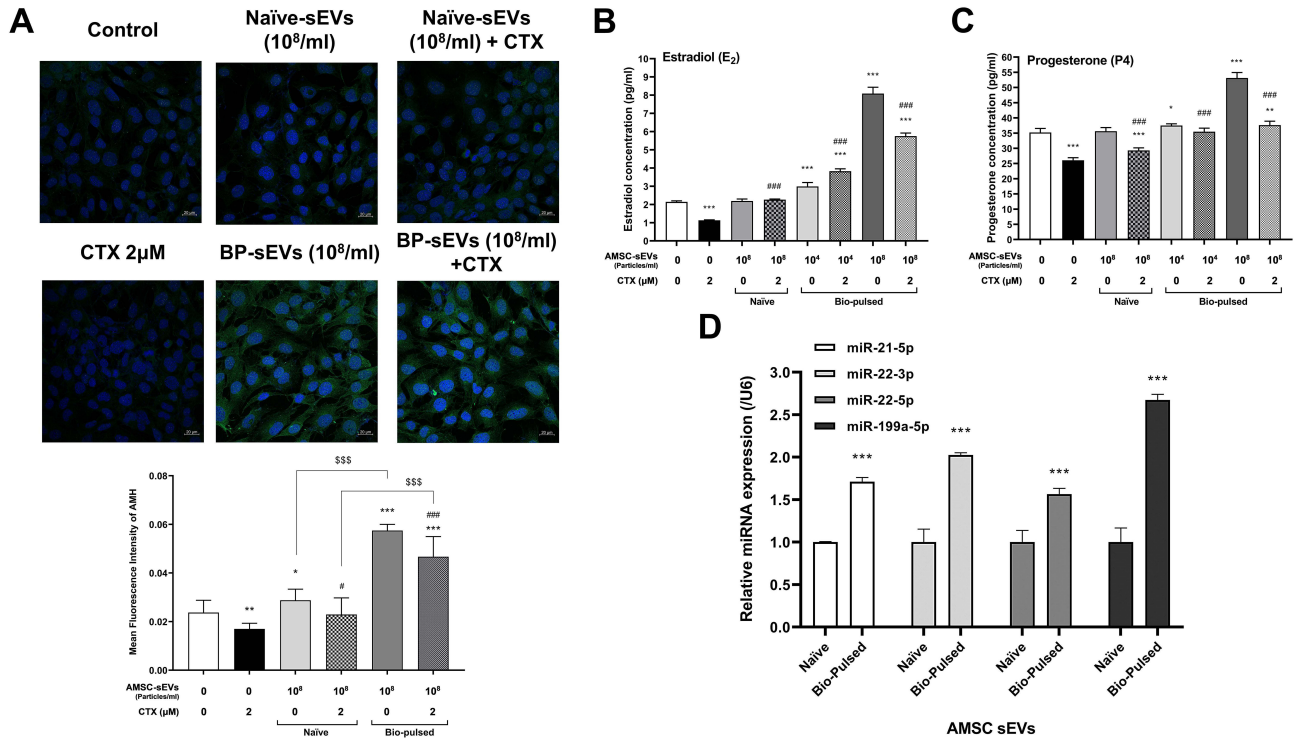

Figure 6 Primed AMSC-sEVs stimulate and restore CTX-reduced steroidogenesis in hGCs. hGCs were treated with or without 2 μM CTX for 48 h, followed by treatment with naïve or Primed AMSC-sEVs for an additional 48 h. (**A**) AMH protein expression was determined by immunofluorescence staining and laser scanning confocal microscopy. The values reported were obtained from fluorescence analysis of AMH images, which showed in supplementary Figure 1. (N = 4, data are expressed as the mean ± standard deviation; $^{*}p < 0.05$, $^{**}p < 0.01$, $^{***}p < 0.001$, compared with 0 μM and 0 particles/mL; $^{\#}p < 0.05$, $^{\#\#\#}p < 0.001$, compared with CTX 2 μM; $^{\$\$\$}p < 0.001$, compared with naïve AMSC-sEVs) (**B**) Estradiol (E2) and progesterone (P4) secretion in hGCs was measured by ELISA. (N = 6, data are expressed as the mean ± standard deviation; $^{*}p < 0.05$, $^{**}p < 0.01$, $^{***}p < 0.001$, compared with 0 μM and 0 particles/mL; $^{\#\#\#}p < 0.001$, compared with CTX 2 μM) (**C**) The expression of potential steroidogenesis-associated miRNAs in naïve and Primed AMSC-sEVs was analyzed by miRNA qRT-PCR. (N = 3, data are expressed as the mean ± standard deviation; $^{***}p < 0.001$, compared with naïve group.). (**D**) The relative expression of selected miRNAs (miR-21-5p, miR-22-3p, miR-22-5p, and miR-199a-5p) was quantified in naïve and Primed AMSC-sEVs by qRT-PCR, normalized to U6. (N = 3, data are expressed as the mean ± standard deviation; *** p < 0.001, compared with naïve group).

significantly and dose-dependently boosted the basal secretion of E2 and P4 in hGCs ($p < 0.05$ or $p < 0.001$), but also significantly and dose-dependently restored the CTX-reduced secretion of these hormones ($p < 0.001$) (Figure 6B and C).

The Potentially Involved miRNAs by Which Primed AMSC-sEVs Stimulate and Restore CTX-Reduced Steroidogenesis in hGCs

Research has also revealed that several miRNAs are involved in steroidogenesis in hGCs, including miRNA-21,[8,9] miRNA-22, miRNA-23b,[9,10] miRNA-145,[10] and miRNA-199a.[11] To evaluate the differences in miRNA profiles between naïve and primed AMSC-sEVs, we performed next-generation sequencing. Table 2 shows that the selected miRNAs — gga-miR-21-5p, gga-miR-22-3p, gga-miR-22-5p, gga-miR-23b-3p, gga-miR-199b, gga-miR-199-3p, gga-miR-199-5p, and gga-miR-145-5p — had significantly higher reads in primed AMSC-sEVs compared to naïve ones ($p < 0.001$). To confirm the fold changes in miRNA expression, we conducted miRNA qRT-PCR analysis on gga-miRNA-21-5p, gga-miRNA-22-3p, gga-miRNA-22-5p, and gga-miRNA-199a-5p in both naïve and primed AMSC-sEVs. The results showed that the expression levels of these miRNAs were significantly increased after priming treatment ($p < 0.001$) (Figure 6D).

Discussion

In the present study, we demonstrated that primed AMSC-sEVs significantly enhanced the proliferation and functional characteristics of hGCs while mitigating CTX-induced cellular damage. These findings support the potential application of primed sEVs as a nanotherapeutic strategy for reproductive disorders such as POI.

Table 2 The Differential Expressed miRNAs (DEMs) in Naïve sEVs and Primed sEVs

DEMs	Reads of miRNA		Log2FC	Regulation	*p*-value
	Naïve sEVs	Primed sEVs			
gga-miR-21-5p	210,645	1,423,493	3.9758	Up	< 0.001
gga-miR-22-3p	35,839	66,549	2.1122	Up	< 0.001
gga-miR-22-5p	194	1,308	3.9725	Up	< 0.001
gga-miR-23b-3p	7,000	93,676	4.9615	Up	< 0.001
gga-miR-199b	433	70,377	8.5639	Up	< 0.001
gga-miR-199-3p	211	68,075	9.5531	Up	< 0.001
gga-miR-199-5p	925	59,526	7.2272	Up	< 0.001
gga-miR-145-5p	175	6,083	6.3386	Up	< 0.001

Priming enhanced both the quantity and quality of AMSC-derived sEVs. According to TRPS analysis, primed sEVs exhibited a higher particle count and narrower size distribution (Figure 1A), indicating improved production efficiency and vesicle uniformity. Correspondingly, primed sEVs significantly promoted hGC proliferation in a dose-dependent manner (Figure 1B), outperforming naïve sEVs, and highlighting their superior bioactivity in vitro.

Moreover, the surface charge of sEVs was notably affected by priming. Zeta potential measurements revealed a significantly more negative charge in primed sEVs (–22.8 to –24.4 mV) compared to naïve sEVs (–13.0 to –13.3 mV), which may enhance their colloidal stability and cellular uptake efficiency through increased electrostatic repulsion and optimized endocytotic interaction under physiological conditions.[14,25] These traits contribute to improved stability in biological environments and may reduce the likelihood of vesicle aggregation. Furthermore, the uniform and smaller vesicle profile of primed sEVs may reflect a shift in biogenesis toward exosome-enriched fractions. The bioactive priming agent used—*Polygonum multiflorum* extract—has previously been shown to modulate EV secretion pathways, potentially via ESCRT or ceramide-dependent mechanisms.[26] These physicochemical alterations are not merely structural; they are functionally relevant. EVs with smaller size (<100 nm) and higher negative surface charge have been reported to exhibit improved tissue penetration, prolonged circulation time, and reduced clearance by the mononuclear phagocyte system.[27–29] Such features enhance biodistribution efficiency and may contribute to superior therapeutic efficacy in vivo. Although the present work focused on i*n vitro* GC restoration, these nanometric improvements suggest that primed AMSC-sEVs possess translational advantages for future reproductive and endocrine therapeutic applications. These physicochemical features, in concert with miRNA cargo enrichment, may synergistically enhance the therapeutic efficacy of primed AMSC-sEVs in restoring GC function.

In the context of CTX-induced POI of hGCs, primed AMSC-sEVs demonstrated a robust ability to restore ovarian function at both cellular and molecular levels. The significant reduction in CTX-induced apoptosis and the enhancement of cell viability in hGCs treated with primed AMSC-sEVs highlight the potential of these vesicles to mitigate chemotherapy-induced ovarian damage (Figure 3). Notably, a slightly higher apoptotic index was observed in the 10^8 primed EV group under baseline (0 μM CTX) conditions compared to the CTX-treated group. This may reflect transient cellular stress due to excessive EV uptake in non-injured cells, which can trigger mild ER or mitochondrial stress. In contrast, CTX-injured cells may preferentially activate anti-apoptotic pathways (eg, miR-21/BCL-2 axis) in response to EVs, resulting in reduced apoptosis. This highlights the dose- and context-dependent nature of EV effects.[30,31]

Primed AMSC-sEVs demonstrated therapeutic potential by restoring key GC functions impaired by CTX. Specifically, treatment reversed the CTX-induced downregulation of *AMH, FSHR*, and *LHCGR* (Figure 4A), and restored E2 and P4 secretion to near-basal or enhanced levels (Figure 6B and C). These findings suggest that primed sEVs exert regenerative effects on steroidogenic capacity, highlighting their translational potential for hormone deficiency conditions. Moreover, apoptosis suppression was evident both transcriptionally and at the protein level. Primed sEVs downregulated TP53 and CASP3 while upregulating BCL-2 expression (Figure 4B), consistent with anti-apoptotic signaling.

Western blot analysis confirmed a marked reduction in cleaved Caspase-3 and Caspase-9, decreased BAX, and preservation of full-length PARP expression (Figure 5). The unchanged Caspase-8 expression indicates that the effect is primarily mediated via the intrinsic (mitochondrial) pathway. These concerted changes suggest that primed AMSC-sEVs mitigate CTX-induced GC apoptosis and promote cellular resilience.

Our findings demonstrate that primed AMSC-sEVs effectively suppress CTX-induced apoptosis in hGCs by down-regulating TP53, CASP3, and BAX, while upregulating BCL-2, resulting in an increased BCL-2/BAX ratio and attenuated cleavage of Caspase-3 and Caspase-9. These results indicate a shift toward cell survival through modulation of the intrinsic mitochondrial apoptotic pathway. This is consistent with previous reports showing that MSC-derived EVs can preserve ovarian function by maintaining mitochondrial integrity, inhibiting cytochrome c release, and reducing oxidative stress, thereby protecting GCs from chemotherapy-induced apoptosis.[32,33] Importantly, the more pronounced anti-apoptotic effects of primed versus naïve AMSC-sEVs suggest that priming augments EV bioactivity, potentially via enrichment of key miRNAs such as miR-21 and miR-145, which are known to regulate both steroidogenesis and apoptotic signaling in ovarian cells.[9,12,34]

The upregulation of specific miRNAs in primed AMSC-sEVs, including miR-21, miR-22, miR-23b, miR-145, and miR-199a (Table 2 and Figure 6D), suggests a molecular mechanism underlying their effects on ovarian function. These miRNAs, known regulators of steroidogenesis and GCs survival, modulate key pathways essential for estrogen and P4 biosynthesis.[8,9] MiR-21, widely recognized for promoting cell survival and proliferation, regulates enzymes critical for estrogen and P4 synthesis, ensuring adequate steroid hormone production.[8,9] MiR-22 influences aromatase expression, fine-tuning sex hormone balance essential for follicular function.[9,10] MiR-23b modulates inflammatory pathways and LHR expression, affecting P4 production during luteinization. MiR-145, while typically linked to apoptosis, regulates cholesterol transport and steroidogenic enzyme expression, influencing estrogen and P4 synthesis.[10] MiR-199a plays a role in cell differentiation and hypoxia responses, supporting follicular maturation and ovulation.[11] These miRNA-mediated regulatory mechanisms likely contribute to the superior efficacy of primed AMSC-sEVs over naïve sEVs, offering potential therapeutic applications for POI and genitourinary syndrome of menopause (GSM), conditions associated with estrogen deficiency.[35–37]

Primed AMSC-sEVs demonstrate notable advantages over naïve EVs. The priming technique enhances both the quantity and quality of sEVs, resulting in a higher particle count and a more uniform size distribution. This uniformity is critical for ensuring consistent and effective delivery of bioactive molecules to target cells. In contrast, primed EVs, while beneficial, typically focus on enhancing specific functions by exposing source cells to certain stimuli, which may not uniformly improve the overall potency of the vesicles.[34,38] Guided and induced EVs are designed to target specific pathways or carry particular cargo, but these methods often require complex engineering and may not yield as robust an increase in overall vesicle production.[39,40] Primed sEVs, by naturally enhancing the intrinsic properties of the vesicles, provide a more straightforward and potentially safer approach to achieving beneficial outcomes. Furthermore, the upregulation of key miRNAs in primed sEVs, which play a critical role in regulating steroidogenesis and other cellular processes, suggests a more holistic enhancement of vesicle efficacy. This broad-based improvement contrasts with the more targeted but potentially limited enhancements seen in other EV modification strategies.

The physiological relevance of the observations made in this study, particularly using the immortalized hGCs (HGL5), warrants further exploration. Although direct evidence from animal models investigating the effects of primed AMSC-sEVs on ovarian function is not yet available, the cellular mechanisms uncovered in our study are strongly supported by existing literature on MSC-EVs. These include the promotion of GC proliferation, reduction of apoptosis, and enhancement of steroidogenesis, all of which are critical to ovarian function.[32,33] Moreover, the miRNA cargo enriched in primed AMSC-sEVs, including miR-21, miR-22, and miR-145, has been previously implicated in regulating steroidogenic pathways and cellular viability. These findings align with prior studies conducted on primary GCs, suggesting that the molecular effects observed in the HGL5 cell model are likely reflective of broader physiological mechanisms. These miRNAs may serve not only as mechanistic effectors but also as potential potency markers for therapeutic sEV formulations. Such markers are critical for the future development of EV-based nanotherapeutics with standardized quality and predictable biological activity.

While the use of HGL5 cells ensures experimental reproducibility, they do not fully replicate the physiology of primary hGCs due to intrinsic biological differences. This commonly encountered limitation in ovarian research arises from ethical constraints and donor variability. Despite this, our results provide a strong mechanistic foundation for further validation. The observed improvements in GC viability, suppression of apoptosis, and restoration of steroidogenesis support the therapeutic potential of primed AMSC-sEVs in ovarian dysfunction.

Given the study's in vitro nature, planned follow-up experiments using CTX-induced POI animal models will be essential to validate these effects in vivo. Additional studies are also warranted in primary human GCs to assess clinical relevance. Although MSC-derived sEVs generally exhibit low immunogenicity, the possibility of immune responses following repeated or high-dose administration requires further evaluation. Likewise, cellular-level functional recovery does not equate to full fertility restoration, which involves coordinated endocrine and systemic regulation.

Importantly, increasing evidence supports that extracellular vesicles from non-human origins, including avian and plant sources, can elicit conserved regulatory effects in mammalian systems through evolutionarily conserved miRNA sequences such as let-7, miR-21, and miR-10.[41–43] In our study, avian-derived primed sEVs modulated apoptosis and steroidogenesis in human GCs, reinforcing their translational potential. This concept of functional cross-species compatibility opens avenues for xenogeneic sEV-based therapies, provided that their safety, potency, and scalability are rigorously addressed.[44,45] By integrating vesicle engineering, endocrine regulation, and conserved miRNA biology, our findings support the development of next-generation EV-based nanotherapeutics for female reproductive health.

Summary

This study demonstrates that primed AMSC-sEVs significantly improve GC function under cyclophosphamide-induced injury. Compared to naïve sEVs, primed vesicles exhibited enhanced physicochemical properties, including higher particle concentration, smaller and more uniform size distribution, and greater colloidal stability. Functionally, they promoted hGC proliferation, restored steroidogenesis, and suppressed apoptosis more effectively. These effects were linked to an enrichment of conserved miRNAs involved in anti-apoptotic and hormone-regulatory pathways. By integrating vesicle engineering with endocrine modulation, our findings support the translational potential of bioactive, primed sEVs as a next-generation nanotherapeutic strategy for preserving fertility and addressing hormonal decline in premature ovarian insufficiency and related reproductive disorders.

Abbreviations

POI, premature ovarian insufficiency; primed AMSC-sEVs, primed avian mesenchymal stem cell-derived small extracellular vesicles; CTX, cyclophosphamide; GSM, genitourinary syndrome of menopause; hGCs, human granulosa cells. E2, estradiol; P4, progesterone. FSHR, follicle-stimulating hormone receptor; LHCGR, luteinizing hormone/choriogonadotropin receptor; AMH, anti-Müllerian hormone; PCNA, proliferating cell nuclear antigen; BCL-2, B cell lymphoma/leukemia type 2; CASP3, cysteine-aspartic acid protease (caspase)-3; TP53, tumor protein p53 (p53); 18S, 18S ribosomal RNA.

Ethics Approval

The experimental protocols of purchased human granulosa cells (HGL5/hGCs) were approved by the Institutional Review Board of the Tri-Service General Hospital and National Defense Medical University (TSGHIRB No. C202405116).

Acknowledgments

The authors sincerely appreciate Mr. Chien-Te Ho, Sales Manager at Normanda Technology of Taiwan Co., Ltd. (Taipei City, Taiwan), for his professional advice. We also extend our heartfelt thanks to Ascension Medical Biotechnology Co., Ltd. and Instrument Center of National Defense Medical University for their full support in providing methods and technology for this study.

Funding

The study was supported in part by grants from the Tri-Service General Hospital (TSGH-E-113265) and Tri-Service General Hospital Penghu Branch (TSGH-PH-E 112015 and TSGH-PH-E 113016).

Disclosure

Co-authors JS S. and YT C. are co-inventors of primed sEVs and shareholders in Ascension Medical Biotechnology CO., LTD. YT C. also serves as the Chief Scientific Officer of the company. Ju-Sheng Shieh, Yu-Tang Chin, Hui-Rong Cheng, Chuang-Yen Huang, and Ya-Yu Hsieh report holding a patent for a method for producing extracellular vesicle; U.S.A Provisional (63/710,610). The remaining authors declare no commercial or financial relationships that could be perceived as potential conflicts of interest.

References

1. Nuovo S, Passeri M, Di Benedetto E, et al. Characterization of endocrine features and genotype–phenotypes correlations in blepharophimosis–ptosis–epicanthus inversus syndrome type 1. *J Endocrinol Investig*. 2016;39(2):227–233. doi:10.1007/s40618-015-0334-3
2. Chang SH, Kim CS, Lee KS, et al. Premenopausal factors influencing premature ovarian failure and early menopause. *Maturitas*. 2007;58(1):19–30. doi:10.1016/j.maturitas.2007.04.001
3. Wang H, Chen H, Qin Y, et al. Risks associated with premature ovarian failure in Han Chinese women. *Reprod Biomed Online*. 2015;30(4):401–407. doi:10.1016/j.rbmo.2014.12.013
4. Salama M, Anazodo A, Woodruff TK. Preserving fertility in female patients with hematological malignancies: a multidisciplinary oncofertility approach. *Ann Oncol*. 2019;30(11):1760–1775. doi:10.1093/annonc/mdz284
5. Kerr JB, Myers M, Anderson RA. The dynamics of the primordial follicle reserve. *Reproduction*. 2013;146(6):R205–15. doi:10.1530/REP-13-0181
6. Zhang Y, Yan Z, Qin Q, et al. Transcriptome Landscape of Human Folliculogenesis Reveals Oocyte and Granulosa Cell Interactions. *Mol Cell*. 2018;72(6):1021–1034e4. doi:10.1016/j.molcel.2018.10.029
7. Xiong Y, Liu T, Wang S, Chi H, Chen C, Zheng J. Cyclophosphamide promotes the proliferation inhibition of mouse ovarian granulosa cells and premature ovarian failure by activating the lncRNA-Meg3-p53-p66Shc pathway. *Gene*. 2017;596:1–8. doi:10.1016/j.gene.2016.10.011
8. Hilker RE, Pan B, Zhan X, Li J. MicroRNA-21 enhances estradiol production by inhibiting WT1 expression in granulosa cells. *J Mol Endocrinol*. 2021;68(1):11–22. doi:10.1530/JME-21-0162
9. Zhang J, Xu Y, Liu H, Pan Z. MicroRNAs in ovarian follicular atresia and granulosa cell apoptosis. *Reprod Biol Endocrinol*. 2019;17(1):9. doi:10.1186/s12958-018-0450-y
10. Xiao S, Du J, Yuan G, Luo X, Song L. Granulosa Cells-Related MicroRNAs in Ovarian Diseases: mechanism, Facts and Perspectives. *Reprod Sci*. 2024;31(12):3635–3650. doi:10.1007/s43032-024-01523-w
11. Song J, Gao L, Yang G, et al. MiR-199a regulates cell proliferation and survival by targeting FZD7. *PLoS One*. 2014;9(10):e110074. doi:10.1371/journal.pone.0110074
12. Sheikhansari G, Aghebati-Maleki L, Nouri M, Jadidi-Niaragh F, Yousefi M. Current approaches for the treatment of premature ovarian failure with stem cell therapy. *Biomedicine Pharmacotherap*. 2018;102:254–262. doi:10.1016/j.biopha.2018.03.056
13. Yang W, Zhang J, Xu B, et al. HucMSC-Derived Exosomes Mitigate the Age-Related Retardation of Fertility in Female Mice. *Mol Ther*. 2020;28(4):1200–1213. doi:10.1016/j.ymthe.2020.02.003
14. Welsh JA, Goberdhan DCI, O'Driscoll L, et al. Minimal information for studies of extracellular vesicles (MISEV2023): from basic to advanced approaches. *J Extracell Vesicles*. 2024;13(2):e12404. doi:10.1002/jev2.12404
15. Gould SJ, Raposo G. As we wait: coping with an imperfect nomenclature for extracellular vesicles. *J Extracell Vesicles*. 2013;2. doi:10.3402/jev.v2i0.20389
16. van Niel G, D'Angelo G, Raposo G. Shedding light on the cell biology of extracellular vesicles. *Nature Rev Mol Cell Biol*. 2018;19(4):213–228. doi:10.1038/nrm.2017.125
17. Zhang Y, Dou Y, Liu Y, et al. Advances in Therapeutic Applications of Extracellular Vesicles. *Int J Nanomedicine*. 2023;18:3285–3307. doi:10.2147/IJN.S409588
18. Gurunathan S, Kang MH, Qasim M, Khan K, Biogenesis KJH. Membrane Trafficking, Functions, and Next Generation Nanotherapeutics Medicine of Extracellular Vesicles. *Int J Nanomedicine*. 2021;16:3357–3383. doi:10.2147/IJN.S310357
19. KV P. Application of "Primed" Mesenchymal Stromal Cells in Hematopoietic Stem Cell Transplantation: current Status and Future Prospects. *Stem Cells Develop*. 2019;28(22):1473–1479. doi:10.1089/scd.2019.0149
20. Shieh JS, Chin YT, Chiu HC, et al. Bio-Pulsed Stimulation Effectively Improves the Production of Avian Mesenchymal Stem Cell-Derived Extracellular Vesicles That Enhance the Bioactivity of Skin Fibroblasts and Hair Follicle Cells. *Int J Mol Sci*. 2022;23(23):15010. doi:10.3390/ijms232315010
21. Lin HY, Yang YN, Chen YF, et al. 2,3,5,4'-Tetrahydroxystilbene-2-O-beta-D-Glucoside improves female ovarian aging. *Front Cell Dev Biol*. 2022;10:862045. doi:10.3389/fcell.2022.862045
22. Tracy SA, Ahmed A, Tigges JC, et al. A comparison of clinically relevant sources of mesenchymal stem cell-derived exosomes: bone marrow and amniotic fluid. *J Pediatr Surg*. 2019;54(1):86–90. doi:10.1016/j.jpedsurg.2018.10.020
23. Vogel R, Savage J, Muzard J, et al. Measuring particle concentration of multimodal synthetic reference materials and extracellular vesicles with orthogonal techniques: who is up to the challenge? *J Extracell Vesicles*. 2021;10(3):e12052. doi:10.1002/jev2.12052
24. Kivioja T, Vähärautio A, Karlsson K, et al. Counting absolute numbers of molecules using unique molecular identifiers. *Nature Methods*. 2012;9(1):72–74. doi:10.1038/nmeth.1778

25. El Andaloussi S, Mäger I, Breakefield XO, Wood MJA. Extracellular vesicles: biology and emerging therapeutic opportunities. *Nat Rev Drug Discovery*. 2013;12(5):347–357. doi:10.1038/nrd3978
26. Willms E, Cabañas C, Mäger I, Wood MJA, Vader P. Extracellular Vesicle Heterogeneity: subpopulations, Isolation Techniques, and Diverse Functions in Cancer Progression. Review. *Front Immunol*. 2018;9. doi:10.3389/fimmu.2018.00738
27. Xu M, Qi Y, Liu G, Song Y, Jiang X, Du B. Size-Dependent In Vivo Transport of Nanoparticles: implications for Delivery, Targeting, and Clearance. *ACS Nano*. 2023;17(21):20825–20849. doi:10.1021/acsnano.3c05853
28. Caponnetto F, Manini I, Skrap M, et al. Size-dependent cellular uptake of exosomes. *Nanomedicine*. 2017;13(3):1011–1020. doi:10.1016/j.nano.2016.12.009
29. Gurunathan S, Kang MH, Jeyaraj M, Qasim M, Kim JH. Review of the Isolation, Characterization, Biological Function, and Multifarious Therapeutic Approaches of Exosomes. *Cells*. 2019;8(4). doi:10.3390/cells8040307
30. O'Brien K, Ughetto S, Mahjoum S, Nair AV, Breakefield XO. Uptake, functionality, and re-release of extracellular vesicle-encapsulated cargo. *Cell Reports*. 2022;39(2):110651. doi:10.1016/j.celrep.2022.110651
31. Mathieu M, Martin-Jaular L, Lavieu G, Théry C. Specificities of secretion and uptake of exosomes and other extracellular vesicles for cell-to-cell communication. *Nature Cell Biol*. 2019;21(1):9–17. doi:10.1038/s41556-018-0250-9
32. Lu Y, Wei Y, Shen X, et al. Human umbilical cord mesenchymal stem cell-derived extracellular vesicles improve ovarian function in rats with primary ovarian insufficiency by carrying miR-145-5p. *J Reprod Immunol*. 2023;158:103971. doi:10.1016/j.jri.2023.103971
33. Liu C, Yin H, Jiang H, et al. Extracellular Vesicles Derived from Mesenchymal Stem Cells Recover Fertility of Premature Ovarian Insufficiency Mice and the Effects on their Offspring. *Cell Transplant*. 2020;29:963689720923575. doi:10.1177/0963689720923575
34. Forsberg MH, Kink JA, Thickens AS, et al. Exosomes from primed MSCs can educate monocytes as a cellular therapy for hematopoietic acute radiation syndrome. *Stem Cell Res Ther*. 2021;12(1):459. doi:10.1186/s13287-021-02491-7
35. Garzon S, Apostolopoulos V, Stojanovska L, Ferrari F, Mathyk BA, Lagana AS. Non-oestrogenic modalities to reverse urogenital aging. *Prz Menopauzalny*. 2021;20(3):140–147. doi:10.5114/pm.2021.109772
36. Brennan A, Brennan D, Rees M, Hickey M. Management of menopausal symptoms and ovarian function preservation in women with gynecological cancer. *Int J Gynecol Cancer*. 2021;31(3):352–359. doi:10.1136/ijgc-2020-002032
37. Calik-Ksepka A, Grymowicz M, Rudnicka E, et al. Signs and symptoms, evaluation, and management of genitourinary tract consequences of premature ovarian insufficiency. *Prz Menopauzalny*. 2018;17(3):131–134. doi:10.5114/pm.2018.78558
38. Noronha NC, Mizukami A, Caliari-Oliveira C, et al. Priming approaches to improve the efficacy of mesenchymal stromal cell-based therapies. *Stem Cell Res Ther*. 2019;10(1):131. doi:10.1186/s13287-019-1224-y
39. Yu T, Xu Q, Chen X, et al. Biomimetic nanomaterials in myocardial infarction treatment: harnessing bionic strategies for advanced therapeutics. *Mater Today Bio*. 2024;25:100957. doi:10.1016/j.mtbio.2024.100957
40. Tan SHS, Wong JRY, Sim SJY, et al. Mesenchymal stem cell exosomes in bone regenerative strategies-a systematic review of preclinical studies. *Mater Today Bio*. 2020;7:100067. doi:10.1016/j.mtbio.2020.100067
41. MJCv H, Driedonks TAP, Snoek BL, et al. Abundantly Present miRNAs in Milk-Derived Extracellular Vesicles Are Conserved Between Mammals. Brief Research Report. *Frontiers in Nutrition*. 2018;5. doi:10.3389/fnut.2018.00081
42. Shi L, Guo C, Fang M, Yang Y, Yin F, Shen Y. Cross-kingdom regulation of plant microRNAs: potential application in crop improvement and human disease therapeutics. *Front Plant Sci*. 2024;15:1512047. doi:10.3389/fpls.2024.1512047
43. Zhang L, Hou D, Chen X, et al. Exogenous plant MIR168a specifically targets mammalian LDLRAP1: evidence of cross-kingdom regulation by microRNA. *Cell Research*. 2012;22(1):107–126. doi:10.1038/cr.2011.158
44. Seegobin N, Taub M, Vignal C, et al. Small milk-derived extracellular vesicles: suitable vehicles for oral drug delivery? *Eur J Pharm Biopharm*. 2025;212:114744. doi:10.1016/j.ejpb.2025.114744
45. Samuel M, Fonseka P, Sanwlani R, et al. Oral administration of bovine milk-derived extracellular vesicles induces senescence in the primary tumor but accelerates cancer metastasis. *Nat Commun*. 2021;12(1):3950. doi:10.1038/s41467-021-24273-8